Electronic Supplementary Material (ESI) for Journal of Materials Chemistry A.
This journal is © The Royal Society of Chemistry 2022

Supporting Information

Hydrogen Bonding Mediated Spillover Enabling Superior Alkaline Industrial-Level Current Density Hydrogen Evolution

Hongyin Hu[a,†], Linsen Zhou[b,†], Fang Duan[a], Han Zhu[a], Hongwei Gu[c], Shuanglong Lu*[a], Mingliang Du[a]

[a] Key Laboratory of Synthetic and Biological Colloids, Ministry of Education, School of Chemical and Material Engineering, Jiangnan University, Wuxi 214122, P. R. China.

[b] Institute of Materials, China Academy of Engineering Physics, Mianyang 621907, P. R. China.

[c] Key Laboratory of Organic Synthesis of Jiangsu Province, College of Chemistry, Chemical Engineering and Materials Science & Collaborative Innovation Centre of Suzhou Nano Science and Technology, Soochow University, Suzhou 215123, P.R. China.

*Correspondence: Email: lushuanglong@jiangnan.edu.cn (S. L.)

† These authors contributed equally to this work

Contents

1 Materials and Methods **4**

2 Supporting Figures **7**

Figure S1 Optimized geometries of H (a–c), F (d–f), and OH (g–i) adsorbed on Pt(111) surface. 7

Figure S2 Optimized geometries of H (a–d) and OH (e–f) adsorbed on 1F–Pt(111) surface. The dotted lines label those short distances between H and F atoms in angstrom. 7

Figure S3 Optimized geometries of H (a–b) and OH (c–d) adsorbed on 2F–Pt(111) surface. The dotted lines label those short distances between H and F atoms in angstrom. 8

Figure S4 Optimized geometries of H (a–b) and OH (c–d) adsorbed on 3F–Pt(111) surface. The dotted lines label those short distances between H and F atoms in angstrom. 8

Figure S5 Optimized geometries of H (a–b) and OH (c) adsorbed on 8F–Pt(111) surface. The dotted lines label those short distances between H and F atoms in angstrom. 8

Figure S6 Optimized geometries of H_2O on top sites of nF–Pt(111) surfaces with n=0 (a), 1 (b), 2(c), 3(d), and 8(e). The dotted lines label those short distances between H and F atoms in angstrom. 9

Figure S7 TEM of *in-situ* F–Pt NCs. 9

Figure S8 HAADF-STEM image of *in-situ* F–Pt NCs. 10

Figure S9 HRTEM of *in-situ* F–Pt NCs. 10

Figure S10 EDS elemental mapping of *in-situ* F–Pt NCs. 11

Figure S11 TEM of *in-situ* Pt NCs without any F. 11

Figure S12 TEM of *ex-situ* F–Pt/C. 12

Figure S13 TEM of commercial Pt/C. 12

Figure S14 Line-scan EDS elemental distribution of *ex-situ* F–Pt/C. 13

Figure S15 Chronoamperometric curves of *in-situ* F–Pt NCs at a current density near 2 A cm^{-2} for 24 h. 13

Figure S16 TEM of F–Pt NCs after 24h *i-t* test under the high current density near 1 A cm^{-2}. 14

Figure S17 TEM of commercial Pt/C after 24h *i-t* test under the high current density near 1 A cm^{-2}. 14

Figure S18 Six sampling points on F–Pt NCs catalyst were selected to measure the atomic ratio of F-Pt NCs after *i-t* test. 15

Figure S19 Cyclic voltammetry curves of (a) *in-situ* F–Pt NCs, (b) *in-situ* Pt NCs, (c) commercial Pt/C and (d) *ex-situ* F-Pt/C in N_2-saturated 1 M KOH with a scan rate of 50 mV s^{-1}. 16

Figure S20 CO stripping voltammograms of (a) F–Pt NCs, (b) Pt NCs, (c) Pt/C and (d) F–Pt/C in 0.1 M $HClO_4$ with a scan rate of 20 mV s^{-1}. 16

Figure S21 ECSA of *in-situ* F–Pt NCs, *in-situ* Pt NCs and commercial Pt/C measured by H_{upd} and CO stripping. 17

Figure S22 ECSA of *ex-situ* F–Pt/C and commercial Pt/C measured by H_{upd} and CO stripping. 17

Figure S23 XPS spectrum of F1s for *ex-situ* F–Pt/C catalyst. 18

Figure S24 XPS spectrum of Pt4f for *in-situ* F–Pt NCs after *i-t* test. 18

Figure S25 EDS spectra of ex-situ F–Pt/C. 19

Figure S26 EDS spectra of *ex-situ* F-Pt/C catalyst after i-t test. 19

3 Supporting Tables 20

Table S1 Adsorption energies (in eV, $E_{ads}=E_{total}-E_{surface}-E_{gas}$), referenced to gas species and 1/2 molecule (1/2 H_2 and 1/2 F_2 in parentheses) in the gas phase for various adsorbates on pure Pt (111) surface. 20

Table S2 Adsorption energies (in eV, $E_{ads}=E_{total}-E_{surface}-E_{gas}$), referenced to gas species and 1/2 molecule (1/2 H_2 in parentheses) in the gas phase for various adsorbates on 1F–Pt(111) surface. 20

Table S3 Adsorption energies (in eV, $E_{ads}=E_{total}-E_{surface}-E_{gas}$), referenced to gas species and 1/2 molecule (1/2 H_2 in parentheses) in the gas phase for various adsorbates on 2F, 3F and 8F–Pt (111) surface. 20

Table S4 The most stable adsorption sites and adsorption energies ($E_{ads,}$ in eV) of H, OH and H_2O on different Pt surfaces (the adsorption energy relative to 1/2 H_2 in parentheses). d_{H-F} is the short distance between F and H atoms. 21

Table S5 Atomic ratio of selected six sampling points on *in-situ* F–Pt NCs catalyst; points 1–4 on the F–Pt NCs and point 5–6 on the carbon support. 21

Table S6 The content of Pt of *ex-situ* F–Pt/C catalyst and commercial Pt/C catalyst measured by ICP. 21

4 References 21

1 Materials and Methods

Chemicals and Materials: Platinum Bis(acetylacetonate) ($Pt(acac)_2$, 98%) was purchased from Shanghai Civi Chemical Technology Co., Ltd, ammonium fluoride (NH_4F, ≥ 96.0%) was purchased from Sinopharm Chemical Reagent Co., Ltd, commercial Pt/C catalyst (20 wt%) was purchased from Shanghai Hesen Electric Co., Ltd., oleylamine (OAm), Vulcan XC-72 carbon and Nafion solution (5 wt%) were purchased from Aladdin Industrial Co., Ltd. All reagents and solvents used in experiments were commercially available and were used without further purification. All solutions used in synthesis and electrochemical experiments were prepared with deionized water.

Synthesis of *in-situ* F-Pt NCs: In a typical synthesis process, $Pt(acac)_2$ (23.7 mg, 0.06 mmol) and NH_4F (203.5 mg, 5.5 mmol) into a glass vial and dissolve in 5 mL OAm. Magnetic stirring for at least 10 h to form a uniform solution (the remaining small amount of NH_4F may not dissolved and does not affect the synthesis process). Subsequently, the glass vial with precursor solution was transferred into a custom pressure-resistant stainless-steel autoclave, which was then filled with H_2 gas (8 bar). The autoclave was heated from room temperature to 165 ℃ and kept at a constant temperature for 6 hours with 20 rpm magnetic stirring. After the reaction is over, collected the black colloidal products and washed them with ethanol/chloroform (v/v = 3/1) at least 5 times.

Synthesis of *in-situ* Pt NCs: In a typical synthesis process, $Pt(acac)_2$ (23.7 mg, 0.06 mmol) into a glass vial and dissolve in 5 mL OAm. Magnetic stirring for at least 10 h to form a uniform solution. Subsequently, the glass vial with precursor solution was transferred into a custom pressure-resistant stainless-steel autoclave, which was then filled with H_2 gas (8 bar). The autoclave was heated from room temperature to 165 ℃ and kept at a constant temperature for 6 hours with 20 rpm magnetic stirring. After the reaction is over, collected the black colloidal products and washed them with ethanol/chloroform (v/v = 3/1) at least 5 times.

Synthesis of *ex-situ* F-Pt/C catalyst: In a typical synthesis process, commercial Pt/C (25 mg) and NH_4F (203.5 mg, 5.5 mmol) into a glass vial and dissolve in 5 mL OAm. Magnetic stirring for at least 10 h to form a uniform solution (the remaining small amount of NH_4F may not dissolved and does not affect the synthesis process). Subsequently, the glass vial with precursor solution was transferred into a custom pressure-resistant stainless-steel autoclave, which was then filled with H_2 gas (8 bar). The autoclave was heated from room temperature

to 165 ℃ and kept at a constant temperature for 6 hours with 20 rpm magnetic stirring. After the reaction is over, collected the black colloidal products and washed them with ethanol/chloroform (v/v = 3/1) at least 5 times.

Characterizations: The morphologies were characterized on a transmission electron microscope (TEM, JEM-2100) at 200 kV. High-resolution transmission electron microscope (HRTEM) and high-angle annular dark-field scanning TEM (HAADF-STEM) were collected on a Tecnai G2 F30S-Twin operated at a voltage of 300 kV, and the same equipment was conducted to obtain elemental mapping and energy-dispersive X-ray spectrometry (EDS) result. Powder XRD experiments were performed on a Bruker D2 PHASER diffractometer equipped with a Cu Kα radiation (λ = 1.5406 Å). X-ray photoelectron spectroscopy (XPS) spectra were performed with a Thermo Scientific ESCALAB 250XI system using an Al Kα radiation.

Electrochemical Measurements: The *in-situ* F-Pt NCs catalyst for the HER was obtained by mixing *in-situ* F-Pt NCs and Vulcan XC-72 carbon. Add 20 wt% of *in-situ* F-Pt NCs and 80 wt% of Vulcan XC-72 carbon into a glass vial. Using cyclohexane as a dispersant, and ultrasound to disperse. After drying, dispersed 5 mg of the catalyst with isopropanol (970 μL) and 5 wt% Nafion solution (30 μL), and ultrasonically form the ink. Then 10 μL ink of different catalysts were coated on the surface of L-type glassy carbon electrode (disk diameter, 3 mm; geometric area, 0.07065 cm^2) and the loading amount of Pt was 0.14 mg cm^{-2}. The preparation methods of *in-situ* Pt NCs, commercial Pt/C and *ex-situ* F-Pt/C catalyst are the same as *in-situ* F-Pt NCs catalyst, except that commercial Pt/C and *ex-situ* F-Pt/C do not need to be mixed with carbon black.

All the electrochemical experiments were recorded on CHI-660H workstation (Shanghai Chenhua) with a classic three-electrode system. The L-type glassy carbon electrode coated with catalyst, carbon rod and $Hg/HgCl_2$ reference electrode were used as working electrode, counter electrode and reference electrode, respectively. The electrolyte was 1 M KOH solution. All potentials were set with the reference of reversible hydrogen electrode (RHE). Linear sweep voltammetry (LSV) was tested with a scan rate of 5 mV s^{-1}. All the polarization curves were obtained with the 95% ohmic potential drop (iR) correction. Stability was evaluated by *i-t* test at near 1 A cm^{-2} current density.

The electrochemically active surface areas (ECSA) are measured by charge required for underpotentially deposited hydrogen (H_{upd}) and CO stripping. The desorption peaks of H_{upd}

from recorded CVs were used to calculate the ECSAs, assuming a charge density of 210 μC cm^{-2} for one monolayer of hydrogen coverage on Pt surface. The ECSAs were calculated from the charge of CO stripping (the first CV) by subtracting the background charge (the second CV), assuming a charge density of 420 μC cm^{-2}.[1, 2]

Computational Methods: All periodic DFT calculations were performed via the Vienna Ab Initio Simulation Package (VASP)[3, 4] with gradient-corrected Perdew-Burke-Ernzerhof (PBE) functional[5]. The projector augmented wave (PAW) method[6] was used to treat interactions between core and valence electrons. The plane wave basis set expansion of valence electrons was cutoff at a kinetic-energy of 400 eV. The optimized lattice parameter of face-centered cubic Pt bulk was 3.967 Å, in good agreement with the reported experimental data of 3.924 Å[7] . The Pt(111) surface was modeled by a 5-layer slab with 3×3 unit cell. A vacuum gap of 15 Å perpendicular to the surface was added to avoid the interaction between periodic images. The Brillouin zone was sampled by a 3×3×1 Monkhorst-Pack k-point mesh[8] , which sufficiently converged the adsorption and barrier energies within 0.05 eV[9]. For the structure optimizations, adsorbed species and the top three atomic layers were allowed to fully relax, while the bottom two layers were fixed at the bulk positions. A Methfessel-Paxton smearing of 0.1 eV was used to improve the convergence. The energies and forces of relaxations were converged to less than 10^{-5} eV and 0.02 eV/Å, respectively. The geometries were optimized via a conjugate-gradient method, and the transition states between initial and final states were searched by the climbing image nudged elastic band (CI-NEB) method[10]. The transition states were further verified by the vibrational frequency analysis with only one imaginary mode. The adsorption energy of pertinent species was computed as, $E_{ad}=E_{tot}-E_{surf}-E_{mol}$, where E_{tot} and E_{surf} are the energies of the total system and surface with/without F atoms, while E_{mol} is the energy of gas H_2O molecule. A more negative value for adsorption energy indicates a stronger adsorption process. The reaction barrier ($E_b=E_{TS}-E_{IS}$) was defined as the energy difference between transition state (TS) and initial state (IS), and the reaction energy ($\Delta E=E_{FS}-E_{IS}$) as the energy difference between the final state (FS) and IS.

2 Supporting Figures

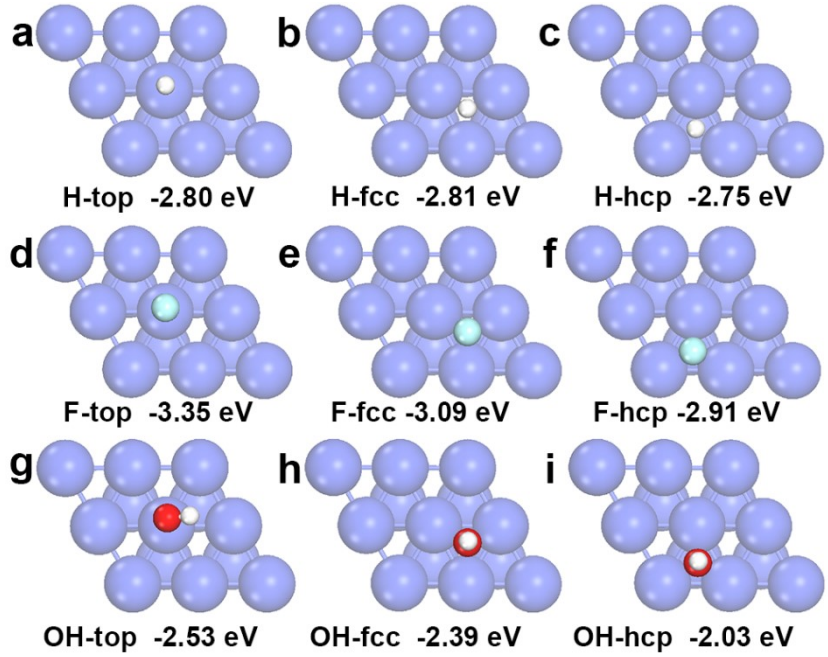

Figure S1 Optimized geometries of H (a-c), F (d-f), and OH (g-i) adsorbed on Pt(111) surface. The purple blue, cyan, white, and red spheres represent Pt, F, H, and O atoms, respectively.

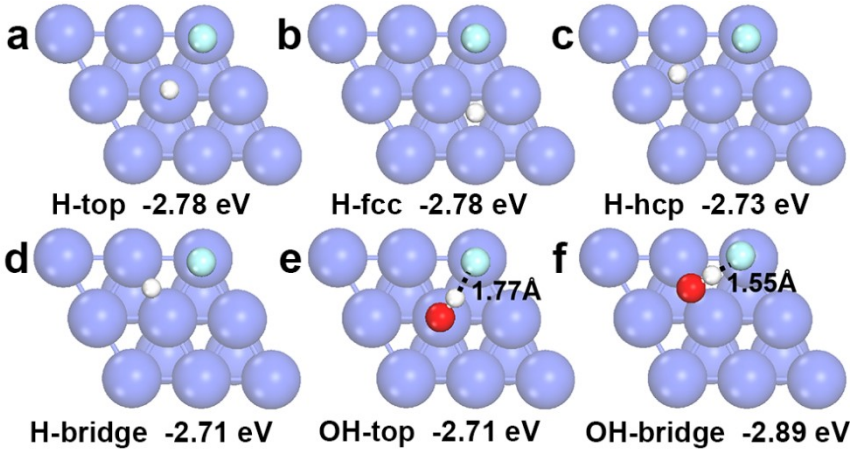

Figure S2 Optimized geometries of H (a-d) and OH (e-f) adsorbed on 1F-Pt(111) surface. The dotted lines label those short distances between H and F atoms in angstrom. The purple blue, cyan, white, and red spheres represent Pt, F, H, and O atoms, respectively.

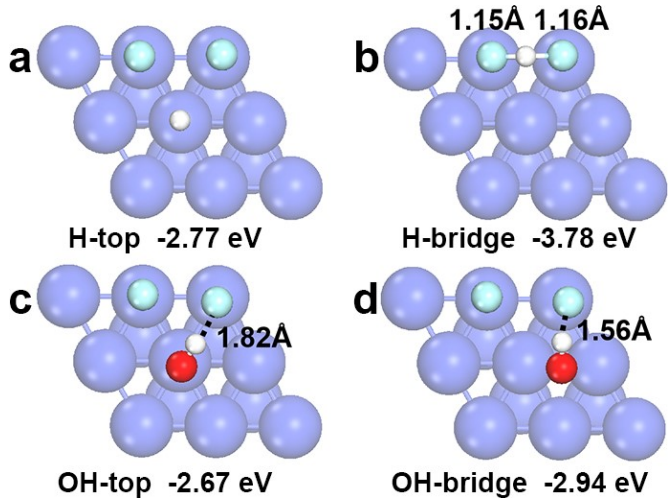

Figure S3 Optimized geometries of H (a-b) and OH (c-d) adsorbed on 2F-Pt(111) surface. The dotted lines label those short distances between H and F atoms in angstrom. The purple blue, cyan, white, and red spheres represent Pt, F, H, and O atoms, respectively.

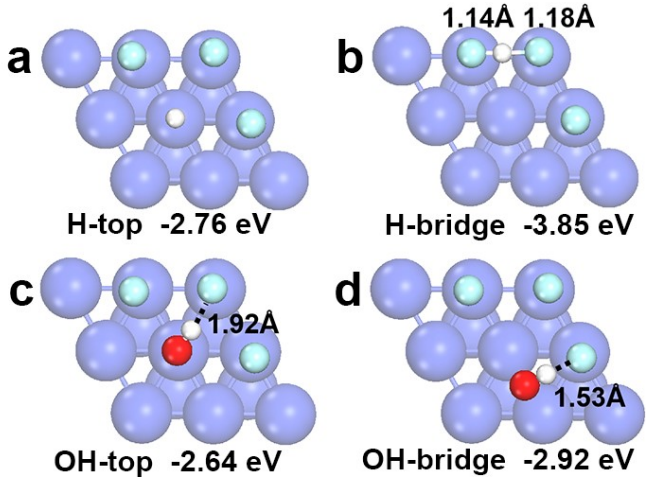

Figure S4 Optimized geometries of H (a-b) and OH (c-d) adsorbed on 3F-Pt(111) surface. The dotted lines label those short distances between H and F atoms in angstrom. The purple blue, cyan, white, and red spheres represent Pt, F, H, and O atoms, respectively.

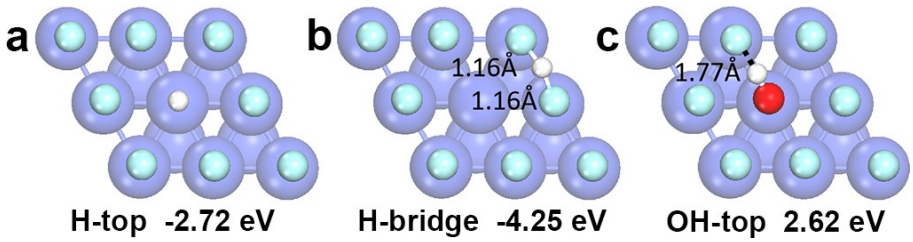

Figure S5 Optimized geometries of H (a-b) and OH (c) adsorbed on 8F-Pt(111) surface. The dotted lines label those short distances between H and F atoms in angstrom. The purple blue, cyan, white, and red spheres represent Pt, F, H, and O atoms, respectively.

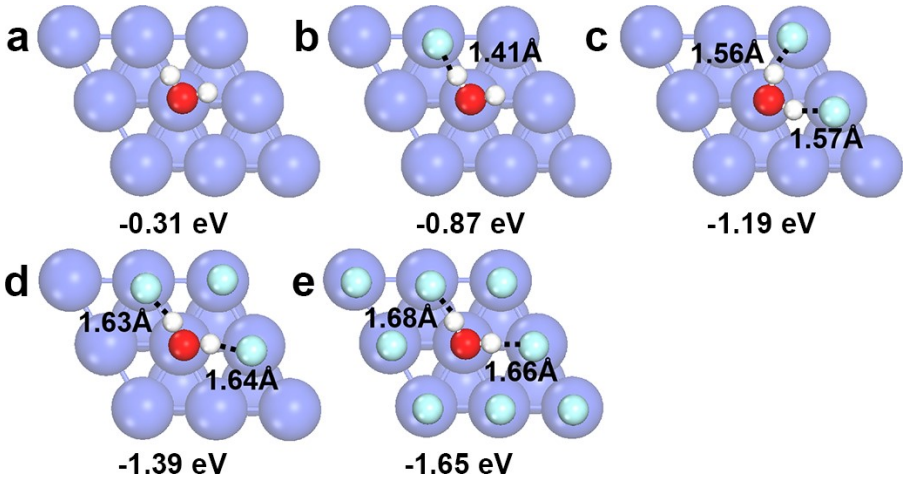

Figure S6 Optimized geometries of H_2O on top sites of *n*F-Pt(111) surfaces with *n*=0 (a), 1 (b), 2(c), 3(d), and 8(e). The dotted lines label those short distances between H and F atoms in angstrom. The purple blue, cyan, white, and red spheres represent Pt, F, H, and O atoms, respectively.

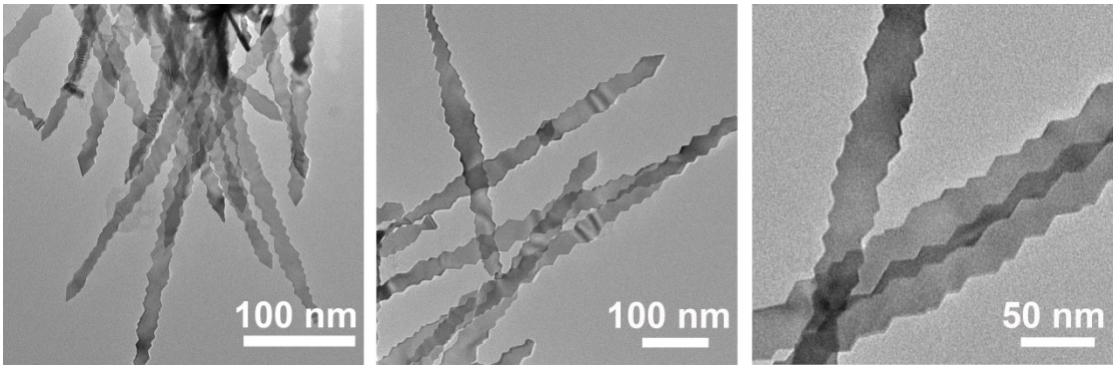

Figure S7 TEM of *in-situ* F-Pt NCs.

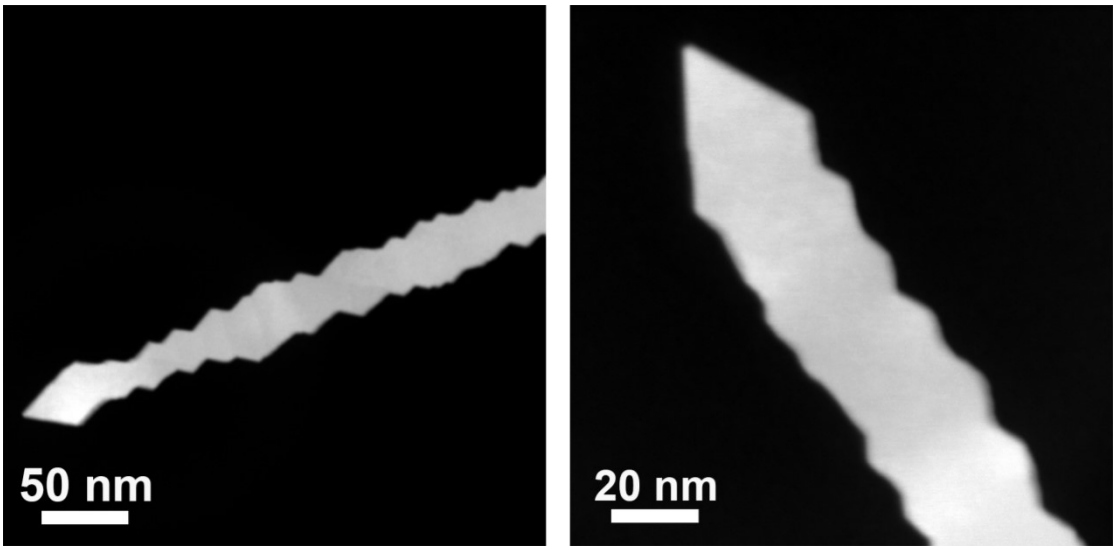

Figure S8 HAADF-STEM image of *in-situ* F-Pt NCs.

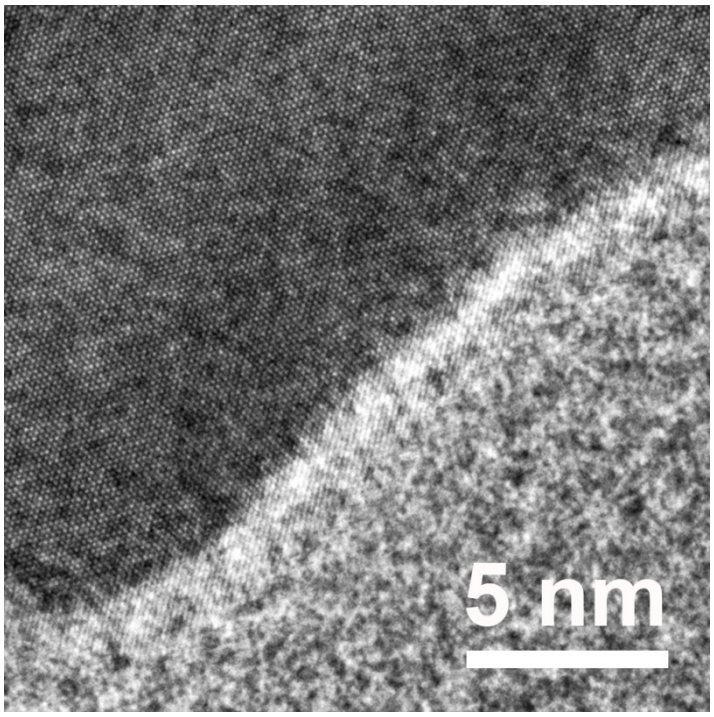

Figure S9 HRTEM of *in-situ* F-Pt NCs.

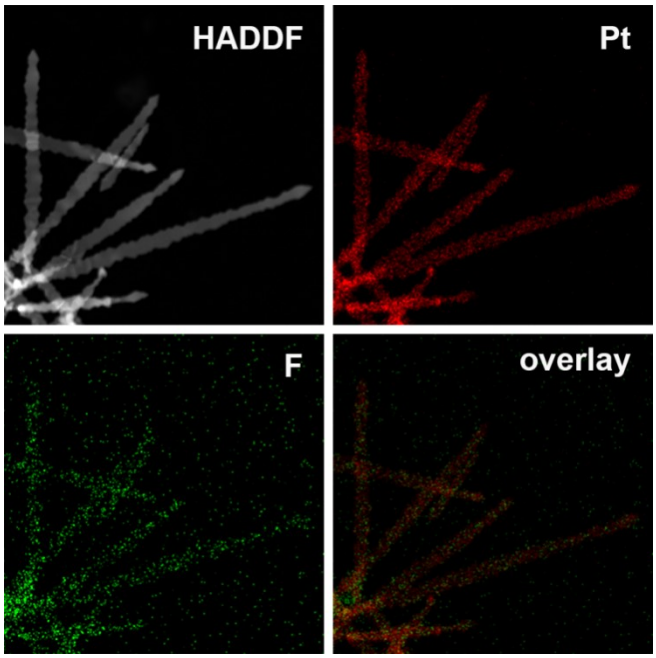

Figure S10 EDS elemental mapping of *in-situ* F-Pt NCs.

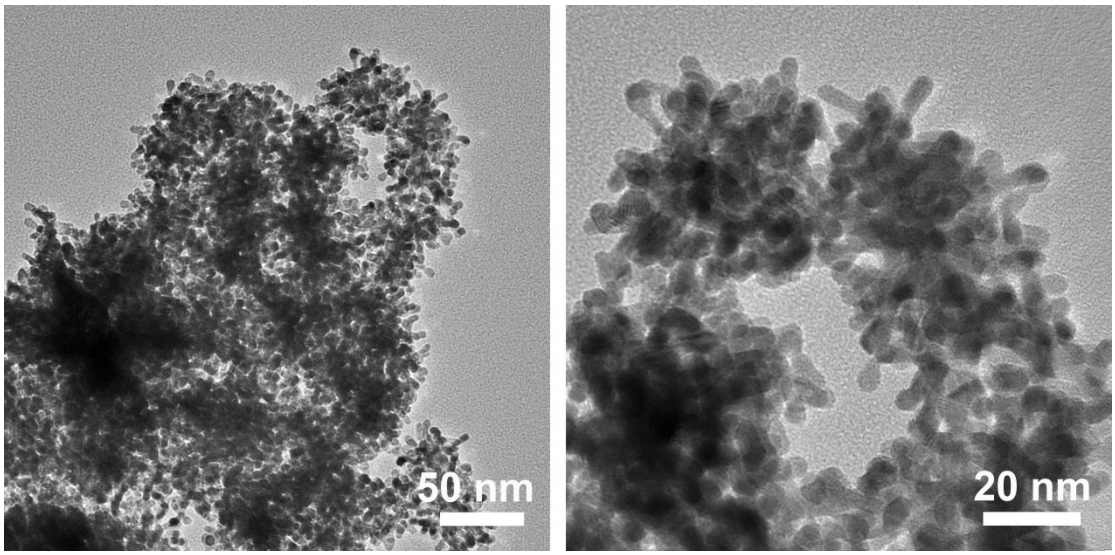

Figure S11 TEM of *in-situ* Pt NCs without any F.

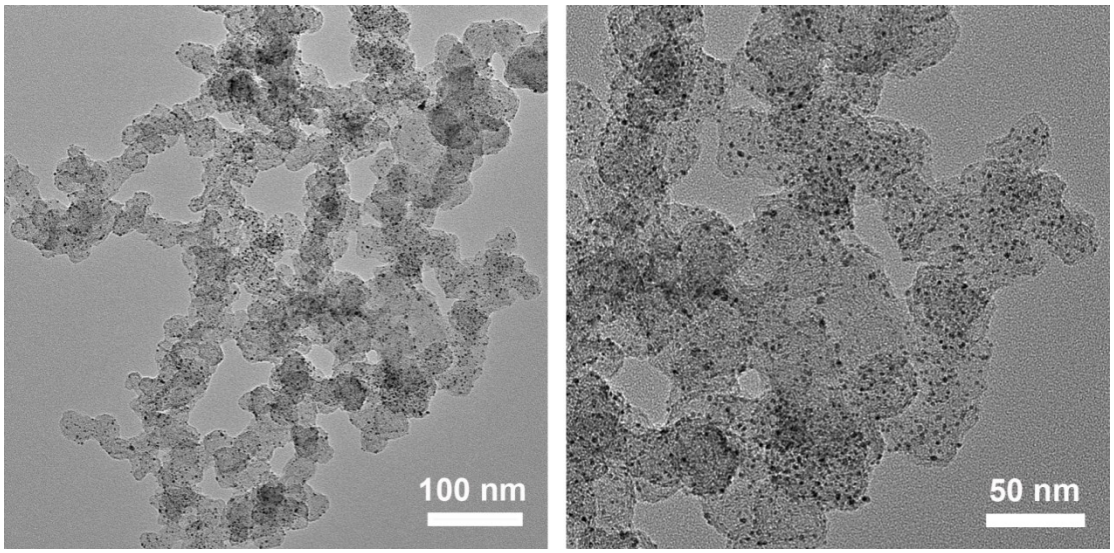

Figure S12 TEM of *ex-situ* F-Pt/C.

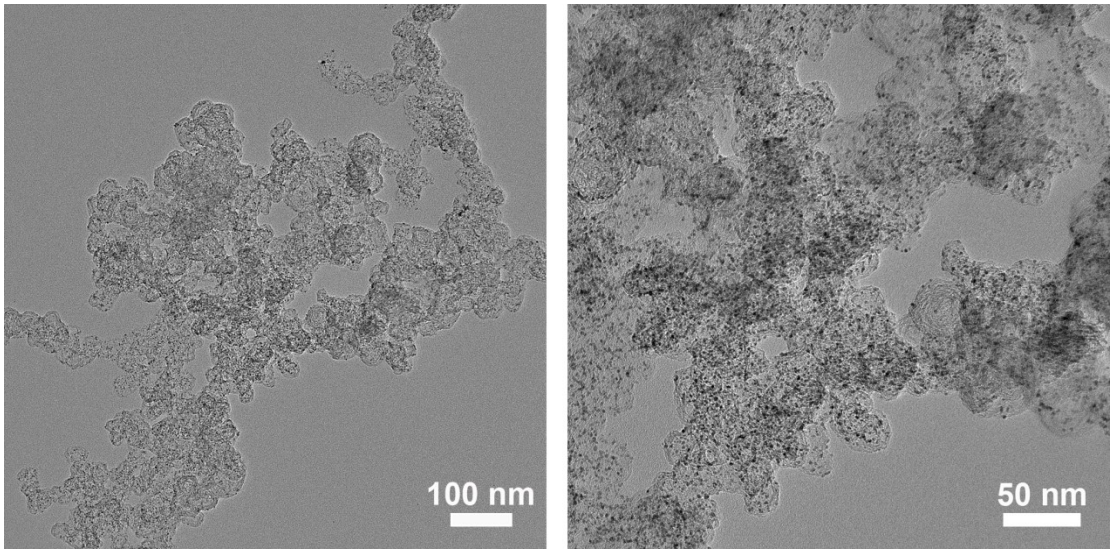

Figure S13 TEM of commercial Pt/C.

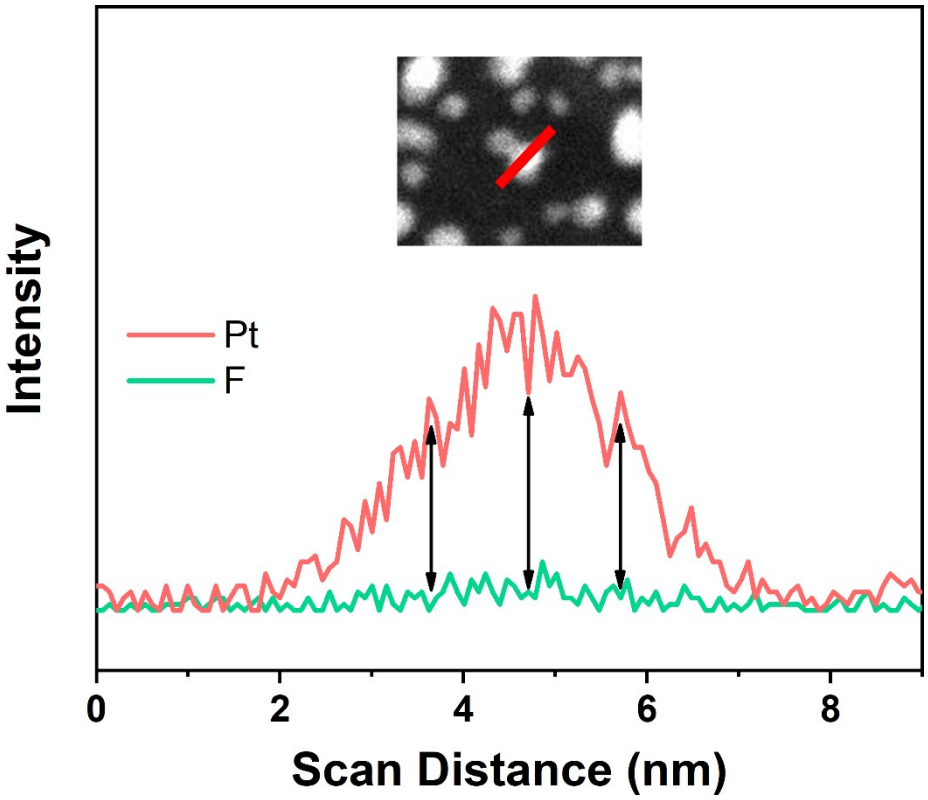

Figure 14 Line-scan EDS elemental distribution of *ex-situ* F-Pt/C.

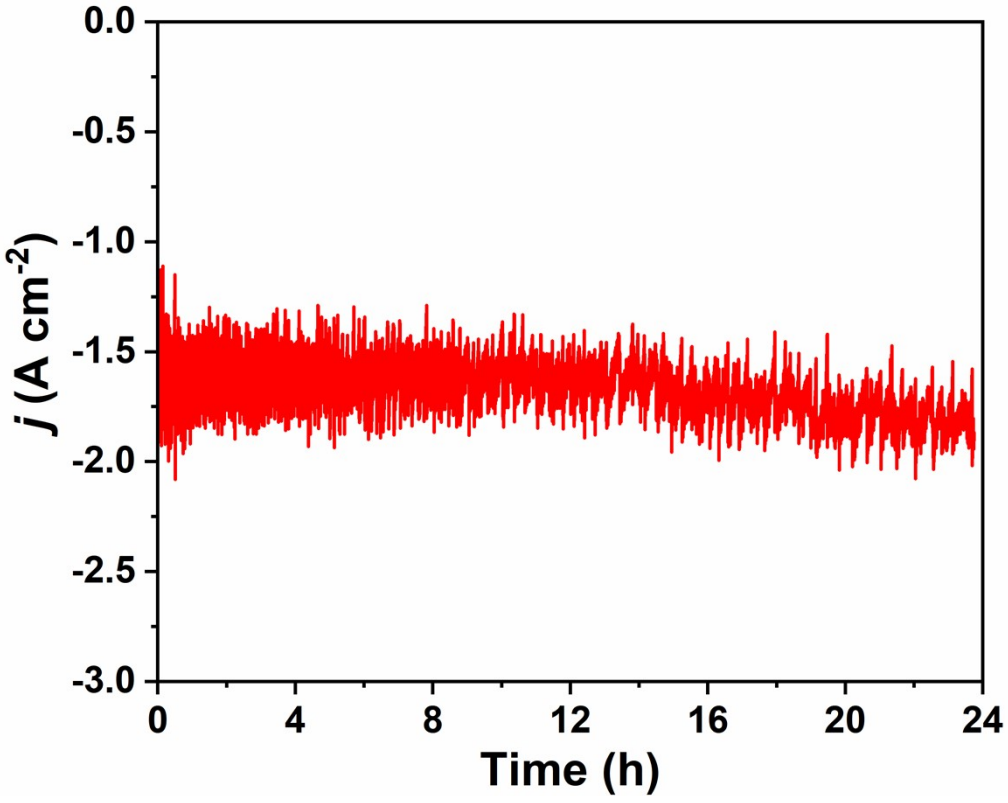

Figure S15 Chronoamperometric curves of *in-situ* F-Pt NCs at an current density near 2 A cm^{-2} for 24 h.

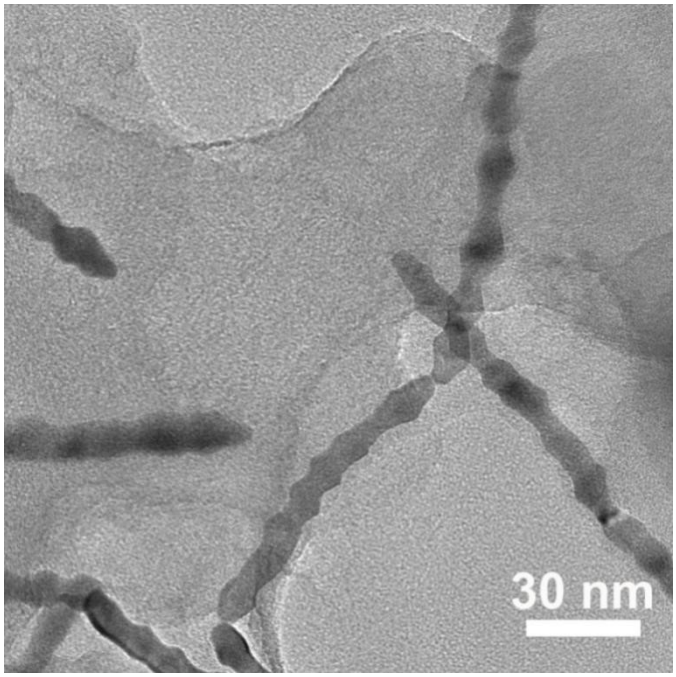

Figure S16 TEM of F-Pt NCs after 24h *i-t* test under the high current density near 1 A cm^{-2}.

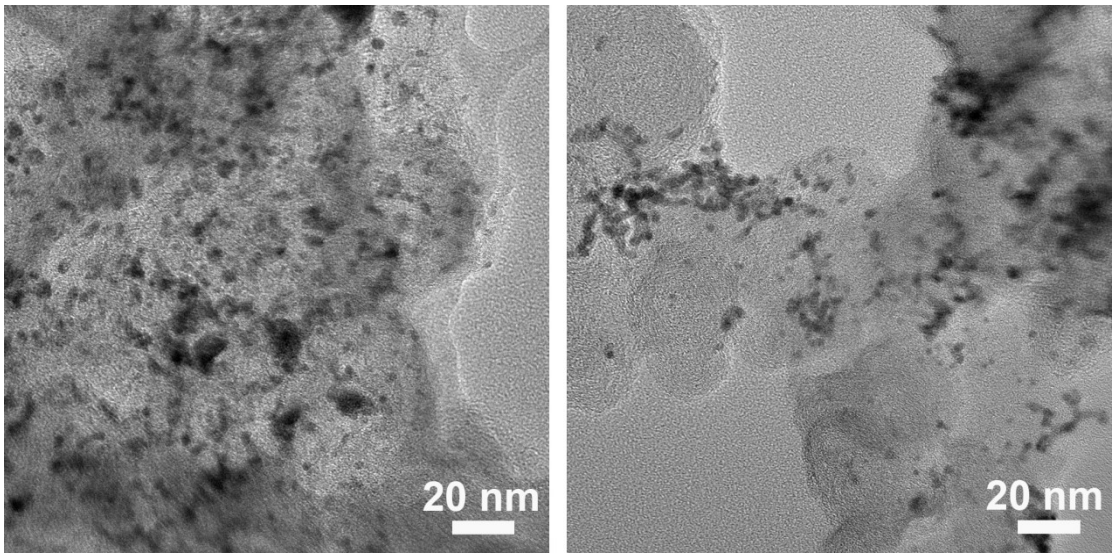

Figure S17 TEM of commercial Pt/C after 24h *i-t* test under the high current density near 1 A cm^{-2}.

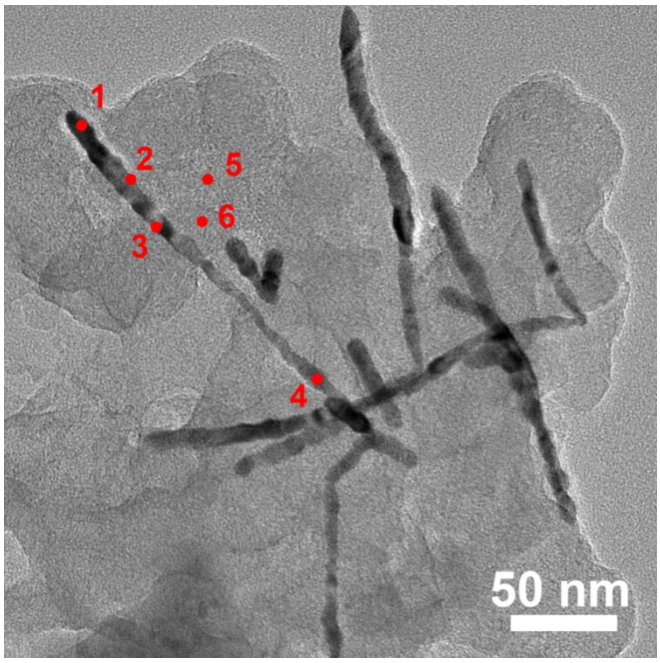

Figure S18 Six sampling points on F-Pt NCs catalyst were selected to measure the atomic ratio of F-Pt NCs after *i-t* test.

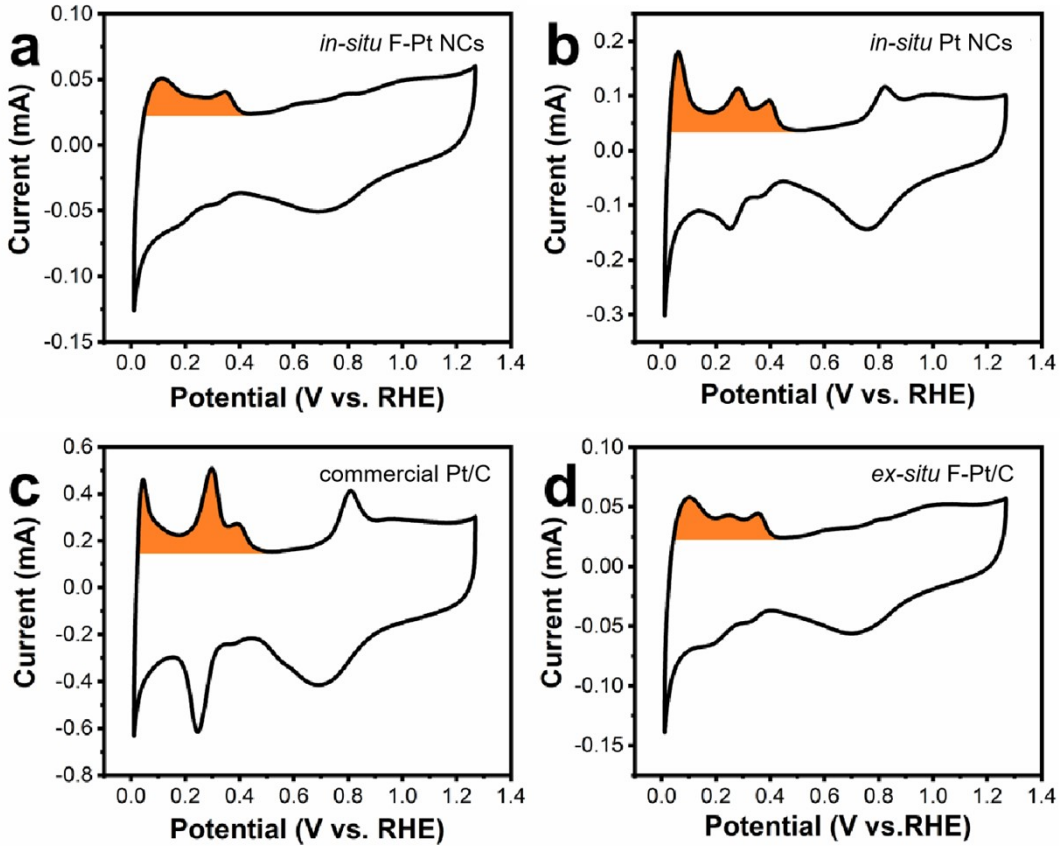

Figure S19 Cyclic voltammetry curves of (a) *in-situ* F-Pt NCs, (b) in-situ Pt NCs, (c) commercial Pt/C and (d) *ex-situ* F-Pt/C in N_2-saturated 1 M KOH with a scan rate of 50 mV s^{-1}.

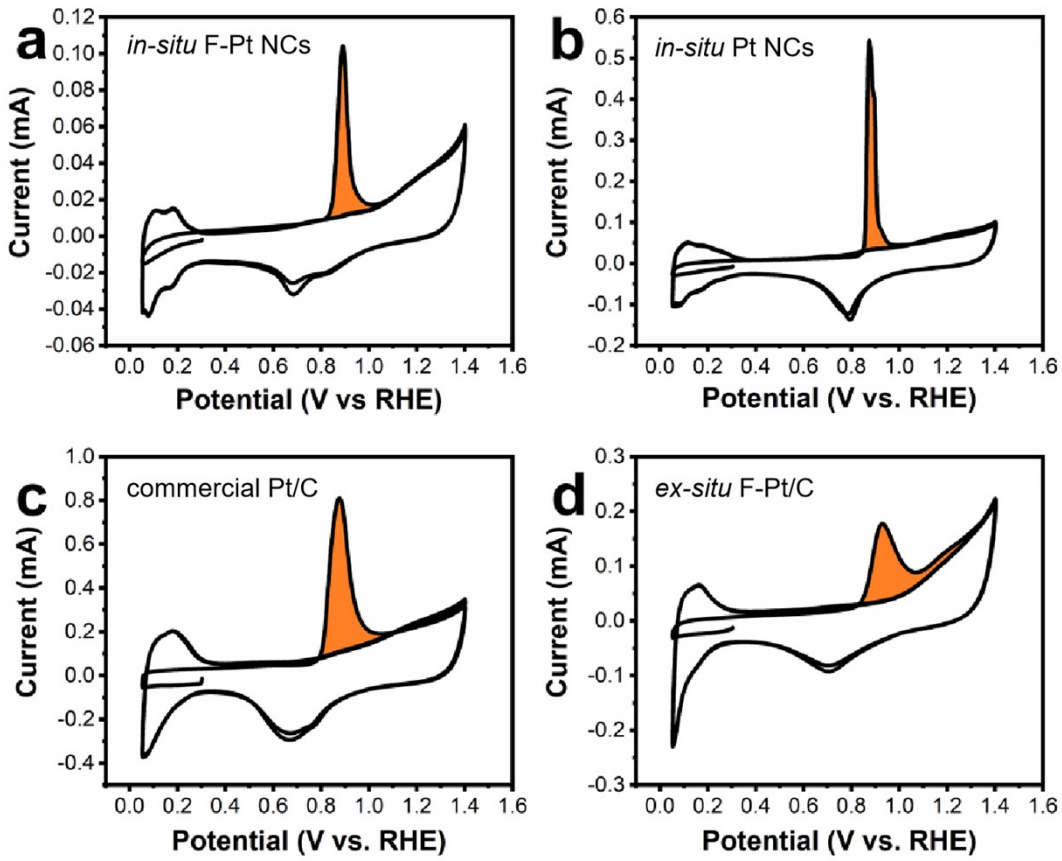

Figure S20 CO stripping voltammograms of (a) F-Pt NCs, (b) Pt NCs, (c) Pt/C and (d) F-Pt/C in 0.1 M $HClO_4$ with a scan rate of 20 mV s^{-1}.

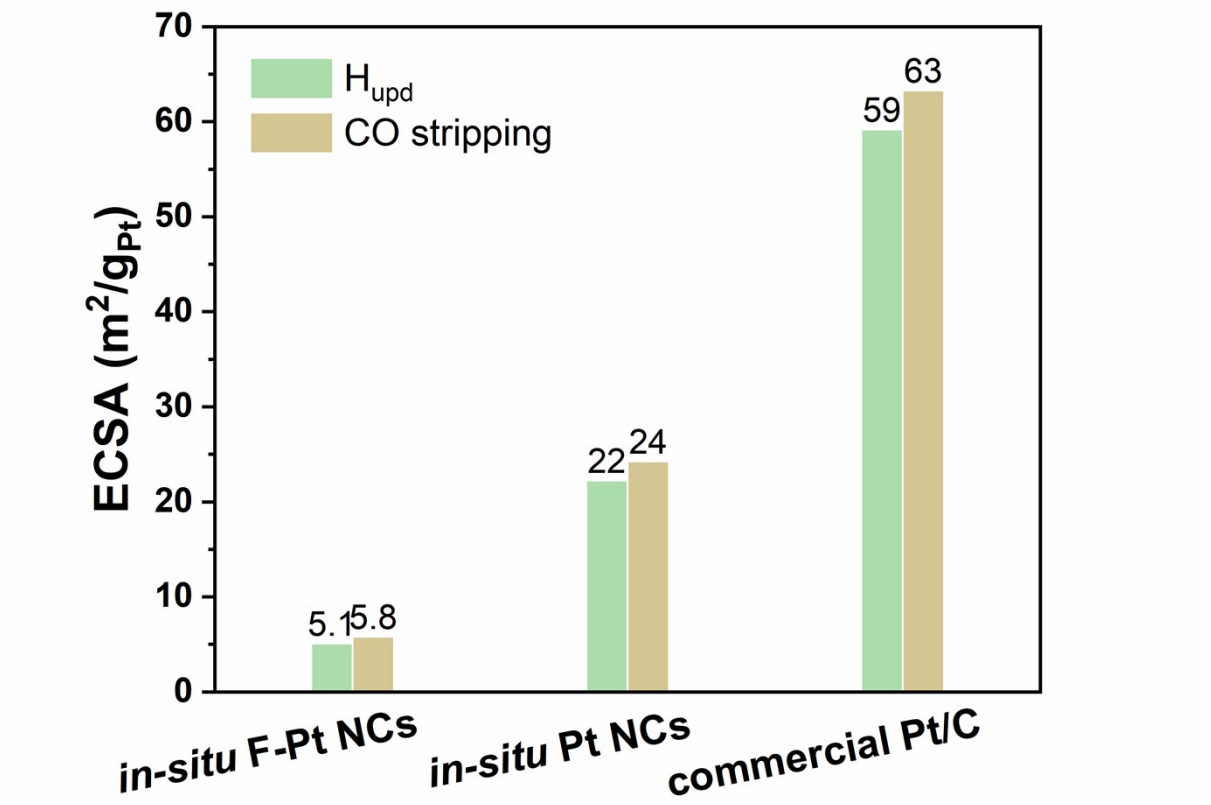

Figure S21 ECSA of *in-situ* F-Pt NCs, *in-situ* Pt NCs and commercial Pt/C measured by H_{upd} and CO stripping.

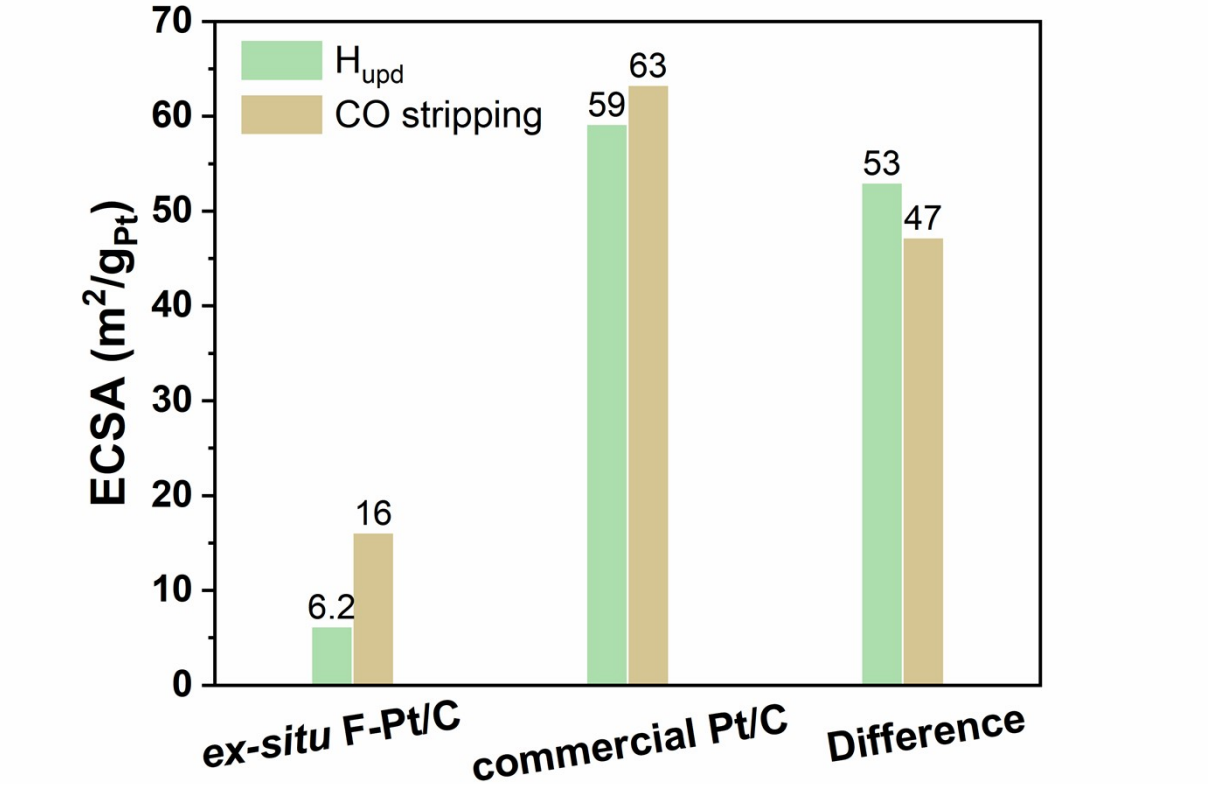

Figure S22 ECSA of *ex-situ* F-Pt/C and commercial Pt/C measured by H_{upd} and CO stripping.

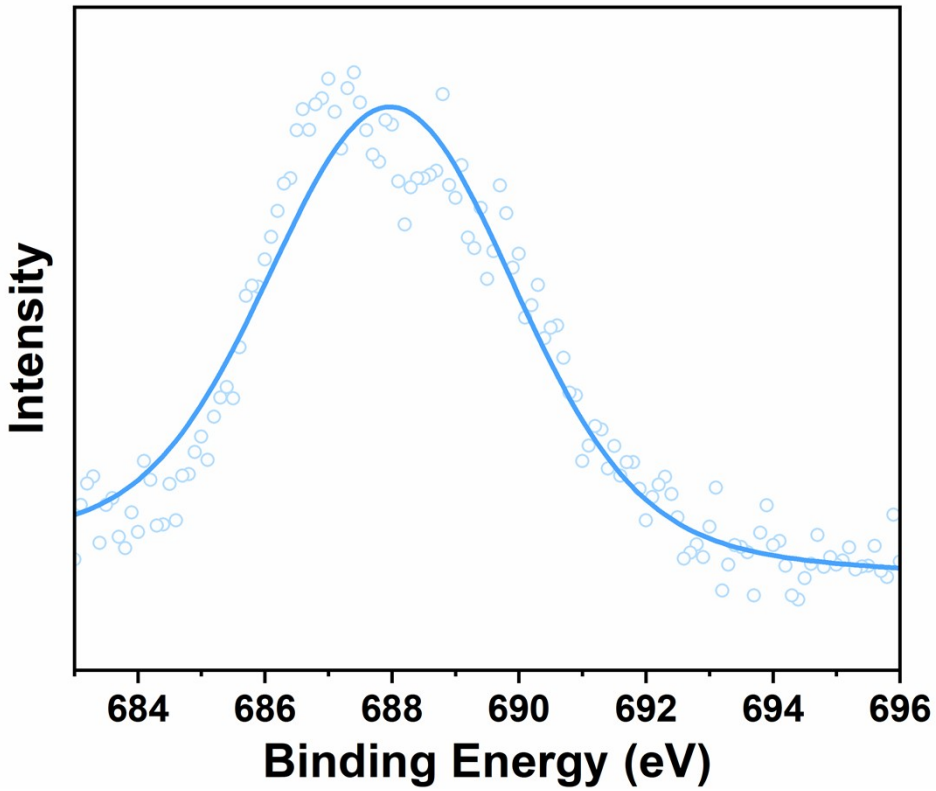

Figure S23 XPS spectrum of F 1s for *ex-situ* F-Pt/C catalyst.

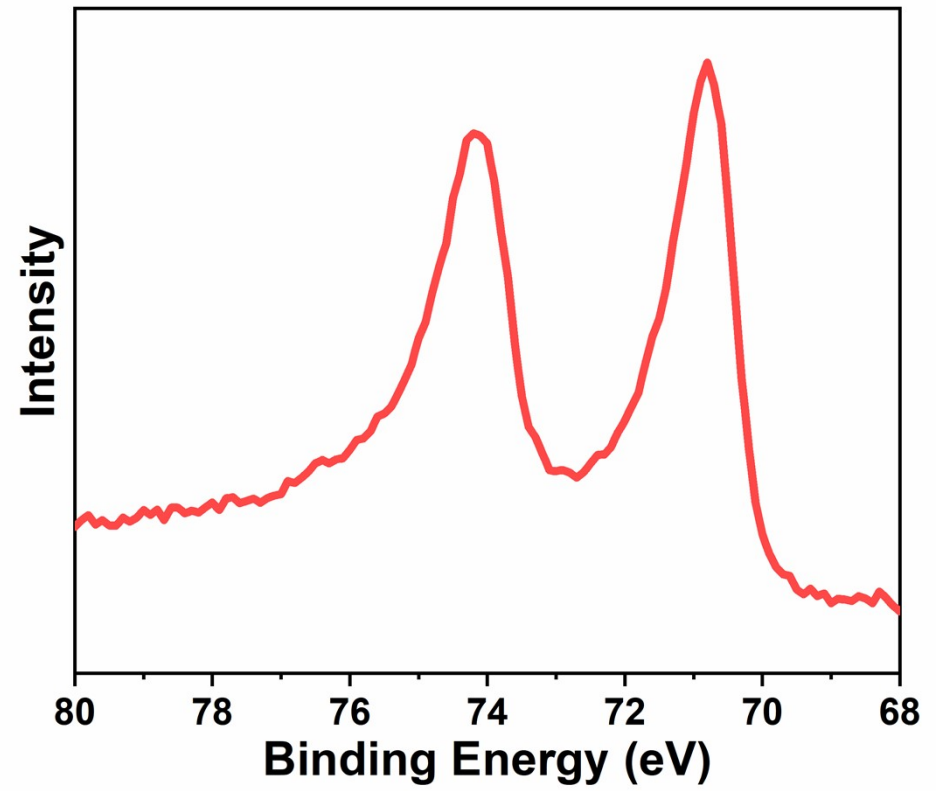

Figure S24 XPS spectrum of Pt 4f for *in-situ* F-Pt NCs after *i-t* test.

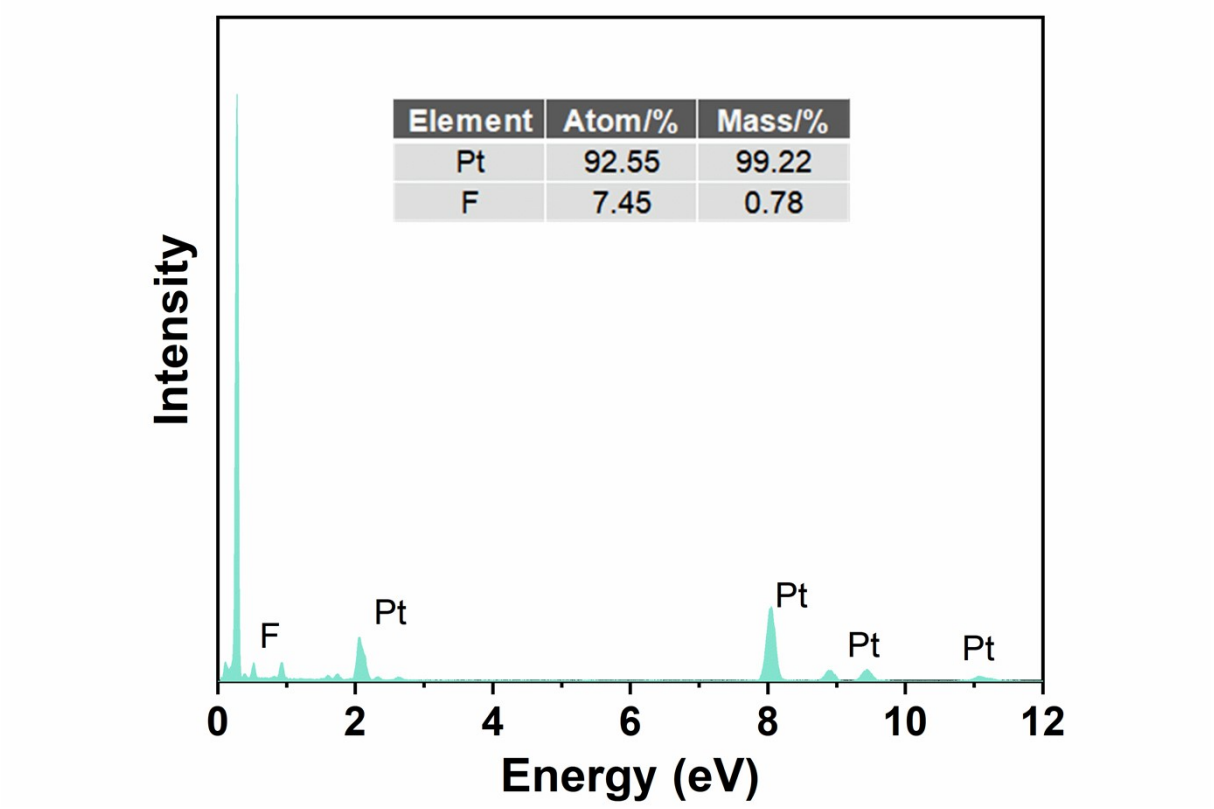

Figure S25 EDS spectra of *ex-situ* F-Pt/C.

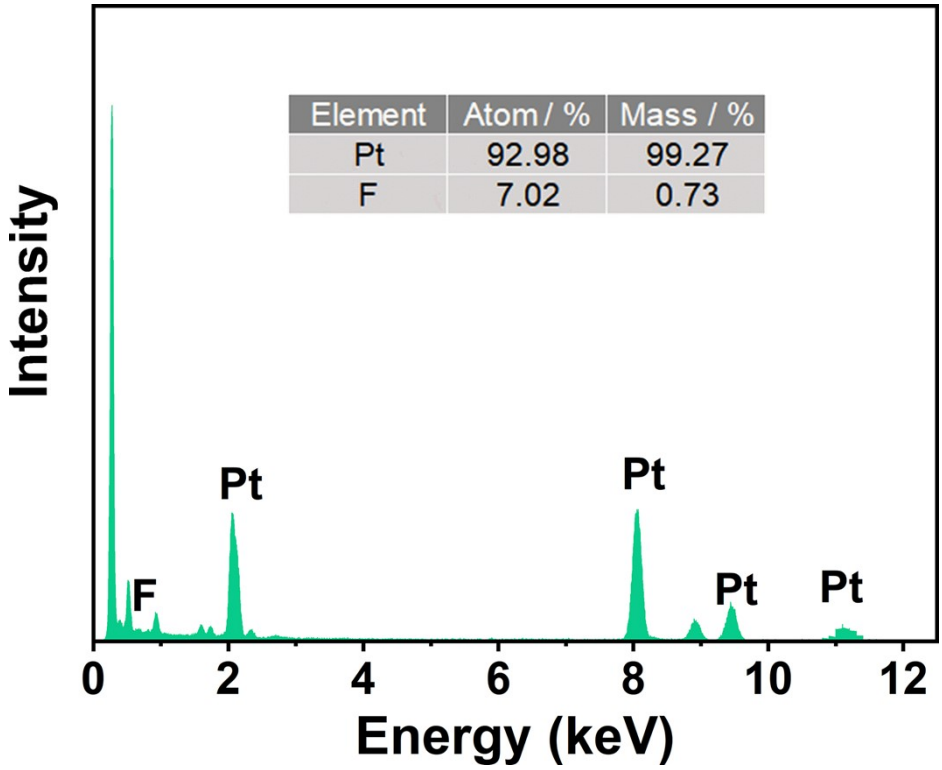

Figure S26 EDS spectra of *ex-situ* F-Pt/C catalyst after i-t test.

3 Supporting Tables

Table S1 Adsorption energies (in eV, $E_{ads}=E_{total}-E_{surface}-E_{gas}$), referenced to gas species and 1/2 molecule (1/2 H_2 and 1/2 F_2 in parentheses) in the gas phase for various adsorbates on pure Pt (111) surface.

species	top	fcc	hcp
H	-2.80 (-0.53)	-2.81 (-0.54)	-2.75 (-0.48)
OH	-2.53	-2.39	-2.03
F	-3.35 (-2.04)	-3.09 (-1.78)	-2.91 (-1.59)

Table S2 Adsorption energies (in eV, $E_{ads}=E_{total}-E_{surface}-E_{gas}$), referenced to gas species and 1/2 molecule (1/2 H_2 in parentheses) in the gas phase for various adsorbates on 1F-Pt(111) surface.

species	top	fcc	hcp	bridge
H	-2.78 (-0.51)	-2.78 (-0.51)	-2.73 (-0.46)	-2.71 (-0.44)
OH	-2.71	---	---	-2.89

Table S3 Adsorption energies (in eV, $E_{ads}=E_{total}-E_{surface}-E_{gas}$), referenced to gas species and 1/2 molecule (1/2 H_2 in parentheses) in the gas phase for various adsorbates on 2F, 3F and 8F-Pt (111) surface.

species	H		OH	
	Top	Bridge (F-F)	top	bridge
2F-Pt(111)	-2.77 (-0.49)	-3.78 (-1.50)	-2.67	-2.94
3F-Pt(111)	-2.76 (-0.48)	-3.85(-1.57)	-2.64	-2.92
8F-Pt(111)	-2.72 (-0.45)	-4.25 (-1.97)	-2.62	---

Table S4 The most stable adsorption sites and adsorption energies (*E*ads, in eV) of H, OH and H_2O on different Pt surfaces (the adsorption energy relative to 1/2 H_2 in parentheses). $d_{H\text{-}F}$ is the short distance between F and H atoms.

species	H			OH			H_2O		
	site	E_{ads} (eV)	$d_{H\text{-}F}$ (Å)	site	E_{ads} (eV)	$d_{H\text{-}F}$ (Å)	site	E_{ads} (eV)	$d_{H\text{-}F}$ (Å)
Pt(111)	Pt3-fcc	-2.81 (-0.54)	---	Pt-top	-2.53	---	Pt-top	-0.31	---
1F-Pt(111)	Pt3-fcc/ Pt-top	-2.78 (-0.51)	2.95/3.44	Pt2-bridge	-2.89	1.55	Pt-top	-0.87	1.41
2F-Pt(111)	F2-bridge	-3.78 (-1.50)	1.15, 1.16	Pt2-bridge	-2.94	1.56	Pt-top	-1.19	1.56, 1.57
3F-Pt(111)	F2-bridge	-3.85 (-1.57)	1.14, 1.18	Pt2-bridge	-2.92	1.53	Pt-top	-1.39	1.63, 1.64
8F-Pt(111)	F2-bridge	-4.25 (-1.97)	1.16, 1.16	Pt-top	-2.62	1.77	Pt-top	-1.65	1.66, 1.68

Table S5 Atomic ratio of selected six sampling points on *in-situ* F-Pt NCs catalyst; points 1-4 on the F-Pt NCs and point 5-6 on the carbon support.

	F	Pt
Point 1	5.06	94.94
Point 2	7.56	92.44
Point 3	0	100
Point 4	0	100
Point 5	0	0
Point 6	0	0

Table S6. The content of Pt in *ex-situ* F–Pt/C and commercial Pt/C catalyst measured by ICP.

Materials	Pt Content in sample 1	Pt Content in sample 2	Average
ex-situ F–Pt/C catalyst	21.51 wt%	21.46 wt%	21.48 wt%
commercial Pt/C catalyst	23.40 wt%	22.91 wt%	23.16 wt%

References

[1] Y. Feng, Q. Shao, Y. Ji, X. Cui, Y. Li, X. Zhu, X. Huang, *Sci. Adv.* **2018,** *4,* eaap8817.

[2] M. Luo, Z. Zhao, Y. Zhang, Y. Sun, Y. Xing, F. Lv, Y. Yang, X. Zhang, S. Hwang, Y. Qin, J.-Y. Ma, F. Lin, D. Su, G. Lu, S. Guo, *Nature* **2019,** *574,* 81.

[3] G. Kresse, J. Furthmuller, *Phys. Rev. B* **1996,** *54,* 11169.

[4] G. Kresse, J. Furthmuller, *Comput. Mater. Sci.* **1996,** *6,* 15.

[5] J. P. Perdew, K. Burke, M. Ernzerhof, *Phys. Rev. Lett.* **1996,** *77,* 3865.

[6] P. E. Blöchl, *Phys. Rev. B* **1994,** *50,* 17953.

[7] Lide, D. R. CRC Handbook of Chemistry and Physics, Internet Version; CRC Press: Boca Raton, FL, 2005.

[8] H. J. Monkhorst, J. D. Pack, *Phys. Rev. B* **1976,** *13,* 5188.

[9] B. Jiang, H. Guo, *J. Phys. Chem. C* **2014,** *118,* 26851.

[10] G. Henkelman, B. P. Uberuaga, H. A. Jónsson, *J. Chem. Phys.* **2000,** *113.* 9901.

[11] T. Imada, M. Chiku, E. Higuchi, H. Inoue, *ACS Catal.* **2020,** *10,* 13718.

[12] Q. Xue, H.-Y. Sun, Y.-N. Li, M.-J. Zhong, F.-M. Li, X. Tian, P. Chen, S.-B. Yin, Y. Chen, *Chem. Eng. J.* **2021,** *421,* 129760.

[13] H. Jin, X. Liu, S. Chen, A. Vasileff, L. Li, Y. Jiao, L. Song, Y. Zheng, S.-Z. Qiao, *ACS Energy Lett.* **2019,** *4,* 805.

[14] H. Jiang, Y. Lin, B. Chen, Y. Zhang, H. Liu, X. Duan, D. Chen, L. Song, *Mater. Today* **2018,** *21,* 602.